Sensors & Actuators: A. Physical 371 (2024) 115273

Contents lists available at ScienceDirect

Sensors and Actuators: A. Physical

journal homepage: www.journals.elsevier.com/sensors-and-actuators-a-physical

Propeller-noise reduction by microfiber coating on a blade surface

Mitsugu Hasegawa , Hirotaka Sakaue *

Department of Aerospace and Mechanical Engineering, University of Notre Dame, Notre Dame, IN 46556, United States

ARTICLE INFO

Keywords:
Microfiber coating
Microstructures
Fibrous surface
Passive noise reduction
Flow control
Propeller noise

ABSTRACT

The popularity of small aerial vehicles has dramatically increased in recent years and propeller noise from such vehicles is a public health concern. Further advancement and utilization of small aerial vehicles require a substantial focus on noise reduction. Microstructures using surface and coating technology are applied in a variety of ways to address this engineering challenge. This study investigates a microfiber coating as a passive means for reducing propeller noise. The microfiber coating is comprised of a fibrous structure and has been previously shown to be a passive mean for reducing drag on a circular cylinder. To begin testing the efficacy of the microfiber coating for propeller noise reduction, microfiber-coated strips are placed at different spanwise locations on propeller blades. The sound pressure level produced by the rotating propeller is measured using a sound-level meter. The microfiber-coated propeller exhibited a lower sound pressure level than that of the uncoated propeller. At a Reynolds number of 7.4×10^4 based on the chord at the 75% spanwise station of the propeller blade, the microfiber-coated propeller achieved a noise reduction of up to 1.6 dBA compared to that of the uncoated propeller. The microfiber coating is effective in reducing broadband noise associated with the interaction of the vortex shedding associated with laminar boundary layer separation. It is found that the noise-reduction performance is a function of the spanwise location of the microfiber-coated strips.

1. Introduction

With the growing popularity of small aerial vehicles such as unmanned aerial vehicles (UAVs) and drones, propeller noise mitigation is a rapidly increasing area of research [1–6]. Propeller noise can be reduced by applying both active and passive flow-control technologies. Passive means utilizing microstructures, such as the use of engineered surfaces, materials, or coatings, are particularly advantageous as they do not require an external power source or mechanical/electrical installation [7]. Serrated leading or trailing edges have been used for noise reduction [8–12]. Alternatively, a furry or a velvet-like surface can be applied to the propeller blade [13–15]. The use of porous treatments has been also investigated to reduce noise sourced from the trailing and leading edge [16,17]. Aerodynamic performance, which is another aspect of propeller characteristics such as thrust force and torque, has been also studied in these studies on passive means. However, the impact on aerodynamic performance is out of focus in the present study.

A microfiber coating comprised of a fibrous structure is the target of the present study. This microfiber coating has been shown to be a passive means for reducing drag on a circular cylinder [18,19]. By applying the microfiber coating to the cylinder, it was found that the vortex behind the cylinder was elongated [20]. It was also found that the fibrous structure suppressed velocity fluctuations around the cylinder [21,22]. Based on these findings, it is hypothesized that the microfiber-induced flow of these features can play a role in reducing propeller noise. The propeller noise is often categorized into tonal noise and broadband noise. The sources of the propeller noise are schematically described in Fig. 1 [7,12,23–28]. These are (A) the interaction of the turbulent boundary layer and the trailing edge known as the turbulent boundary layer trailing-edge noise (TBLTE), (B) vortex shedding associated with the laminar boundary layer and separation bubble known as the laminar boundary layer vortex-shedding noise (LBLVS), (C) the interaction of the propeller blade and the blade-tip vortex known as the blade vortex interaction noise (BVI), and (D) the interaction of the propeller blade and the turbulent wake formed by a preceding blade known as the blade wake interaction noise (BWI). Because these noises are location dependent over the propeller blade, the effect on the microfiber coating will also be location dependent. There is no literature available addressing the effect of propeller noise reduction via microfiber coating. As a first study, this work explores the change in sound pressure level (SPL), which was experimentally obtained in order to study the relationship between propeller noise and the location of the

* Corresponding author.
E-mail address: hsakaue@nd.edu (H. Sakaue).

https://doi.org/10.1016/j.sna.2024.115273
Received 24 November 2023; Received in revised form 1 March 2024; Accepted 12 March 2024
Available online 12 March 2024

microfiber coating. A quadcopter with four propellers was used to simulate practical applications.

2. Experimental setup

2.1. Propeller

Fig. 2 shows a photograph of the propeller (15 × 5.5 MR/MRP, APC, USA) used in the present study. It has a diameter of 381 mm and a pitch of 140 mm. The spanwise location, s, over the propeller is defined as the distance from the rotating center axis toward the blade-tip. At 75% spanwise location relative to the propeller radius, R, the chord length, C, is ~25 mm and the maximum blade thickness, T, is ~2 mm.

The rotating speed of propeller was set at 3000 rpm corresponding to the hovering phase for the quadcopter with this propeller described in Section 2.3. The chord-based Reynolds number, Re, is defined using the velocity and chord at a spanwise station, given by the following equation:

$$\mathrm{Re} = \frac{\rho V C}{\mu} \tag{1}$$

Where ρ represents the air density (kg/m^3), V is the velocity (m/s), C denotes the chord length (m), and μ represents the air dynamic viscosity (kg/(m·s)). The Reynolds number based on the chord at 75% spanwise location was 7.4 × 10^4. Here, the 75% spanwise location is the distance measured from the rotating center axis. Fig. 3 shows the distribution of the chord-based Reynolds number over the blade between $s = 0.47\ R$ to $s = 0.87\ R$. The averaged Reynolds number over the distribution is 7.1 × 10^4, indicating that the laminar boundary layer is dominant over the propeller blade [29,30]. Both a microfiber-coated propeller and uncoated propeller were used in this study. The microfiber-coated propeller has microfiber-coated strips detailed in Section 2.2. The uncoated propeller was used as a baseline for comparison with the microfiber-coated propeller.

2.2. Microfiber-coated strip

Fig. 4(a), (b), and (c) shows a schematic and microscopic images of a fabricated microfiber-coated strip, respectively. It was made using the procedure outlined by Hasegawa *et al.* [31]. Microfibers with an average length of 4.5 mm ± 0.1 mm was used for the fabrication. The diameter of the microfiber was about 50 μm. The microfiber material was Nylon 6/6, Poly (hexamethylene adipamide) from (Campbell Coutts Ltd., Eastleigh, U.K.). The density of the microfiber material was 1.14 g/cm^3. The elastic modulus of the microfiber material was estimated to be 39 ~ 50 GPa [20]. An epoxy adhesive was applied to a film (Simair, U.K.) with a thickness of 50 μm. All microfibers were planted over the adhesive layer and oriented chordwise as shown in Fig. 4(a) and (b). By counting the number of microfibers per unit area on the microscope images, the averaged surface density of the microfiber was found to be 4 fibers/mm^2. The strip had a relative width of 0.28 C and was taped onto the propeller blade. The height of the microfiber-coated strip relative to maximum blade thickness was ~0.5 T.

The microfiber-coated strips were placed at four different spanwise locations. Fig. 5(a) and (b) provide a schematic description of the microfiber-coated strips applied on the propeller blade. The spanwise length of the microfiber-coated strip was 0.13 R. The leeward edges of the microfiber-coated strips were aligned with the trailing edge. As shown in Fig. 5(c), the locations of microfiber-coated strip varied from $s = 0.47\ R$ to $s = 0.87\ R$ along with the span at an interval of 0.13 R. All microfiber-coated strips were applied on the suction side of the propeller blade.

2.3. Quadcopter test stand

The microfiber-coated or uncoated propellers described in Sections 2.1 and 2.2 were mounted on the quadcopter test stand (See Fig. 6(a)). The test stand consists of four components: servo motors, electronic-speed controllers (ESC), rotational-speed transducers, and a quadcopter frame. The servo motors (4014 EEE 370KV, Mad Components) were used to rotate the propellers. The ESC (Xrotor pro 60 A for 4–6 S, Mad Components) was used to control the rotational speed of the four servo motors. The rotational-speed transducers were used to obtain the rotational speed of the rotors. The quadcopter frame (650, Tarot, USA) was attached to a tripod to adjust the quadcopter's ground height. The quadcopter test stand was placed in the anechoic chamber at the Hessert laboratory at the University of Notre Dame (See Fig. 6(b)). A power supply (382275, EXTECH, USA) with a constant voltage was used to stabilize the rotating speed during measurements.

2.4. Noise measurement

Noise around the quadcopter was measured in the anechoic chamber. A sound-level meter (732 A, BK PRECISION, USA) was used to quantify the noise based on sound pressure level (SPL). Fig. 7 shows the schematic description of sound-level meter location. The sound-level meter was placed 2.1 m away from the center of quadcopter test stand in the horizontal direction. The ground height of the sound-level meter

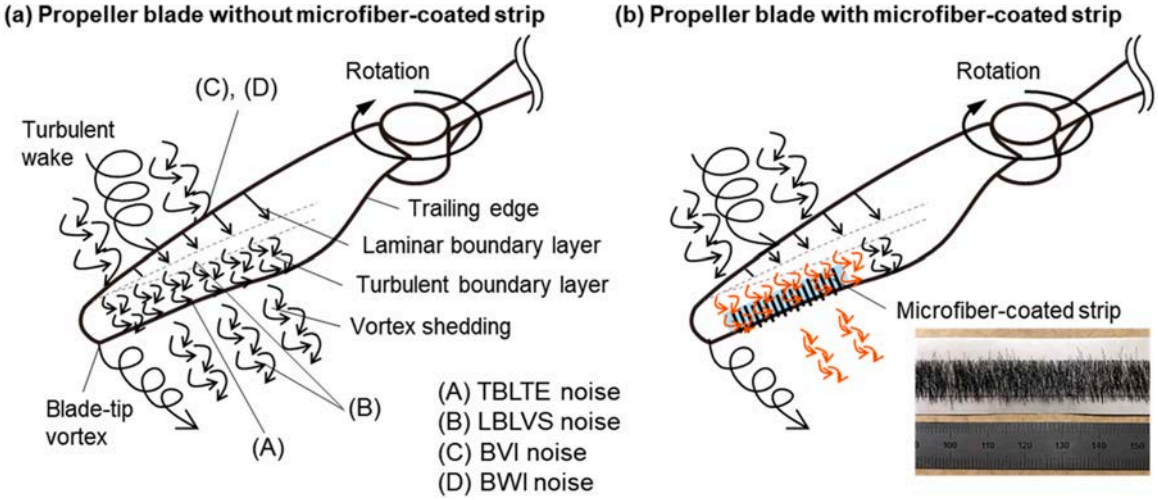

Fig. 1. Schematic descriptions of propeller-noise reduction using the microfiber coating: (a) Propeller blade without microfiber-coated strip; (b) Propeller blade with microfiber-coated strip.

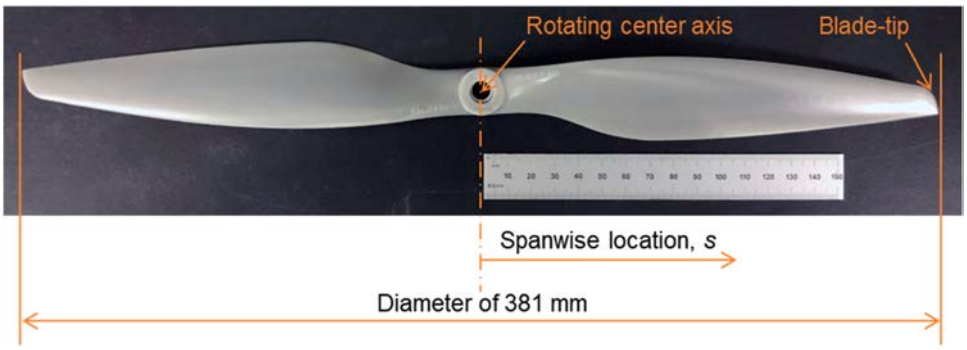

Fig. 2. Photograph of the propeller.

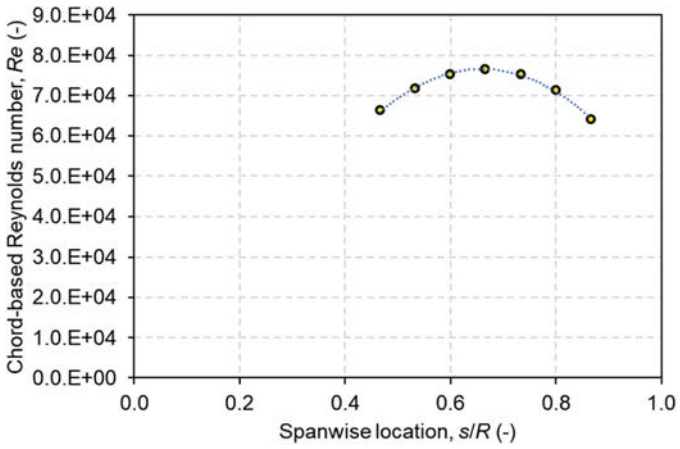

Fig. 3. Distribution of the chord-based Reynolds number over the blade between $s = 0.47\ R$ to $s = 0.87\ R$ in this study.

was 1.3 m. The time-weighted SPL with a time constant of 125 ms was collected for evaluation of the propeller noise described in Section 2.5. The time-weighted SPL was A-weighted to account for the relative loudness perceived by the human ear. The accuracy of the SPL was ±1.5 dB at reference conditions, and the resolution was 0.1 dB. The voltage signal related to the instantaneous sound pressure were also obtained from the sound-level meter so that the frequency spectrum of noise could be studied. The sound-level meter sensitivity is 0.5 V/Pa. The voltage signals were also A-weighted and converted into spectrum components by applying a Fast-Fourier-Transform (FFT), and the logarithmic power spectral density (PSD) in dBA/Hz relative to the reference pressure was computed by using the following equation:

$$\mathrm{PSD} = 10\log_{10}\left(\frac{G}{P_{ref}^2}\right) \tag{2}$$

Where P_{ref} is the reference pressure (20 μPa), and G is the power spectral density from FFT in Pa^2/Hz. Data were sampled at 40 kHz for 25 s. PSD spectrum was averaged over 244 records of 4096 samples each with Hanning window and 50% overlap between records. The frequency resolution was ~10 Hz. Based on the Nyquist criterion, the sampling frequency of 40 kHz allowed for the frequency spectrum up to 20 kHz, which is the upper limit of the human hearing range.

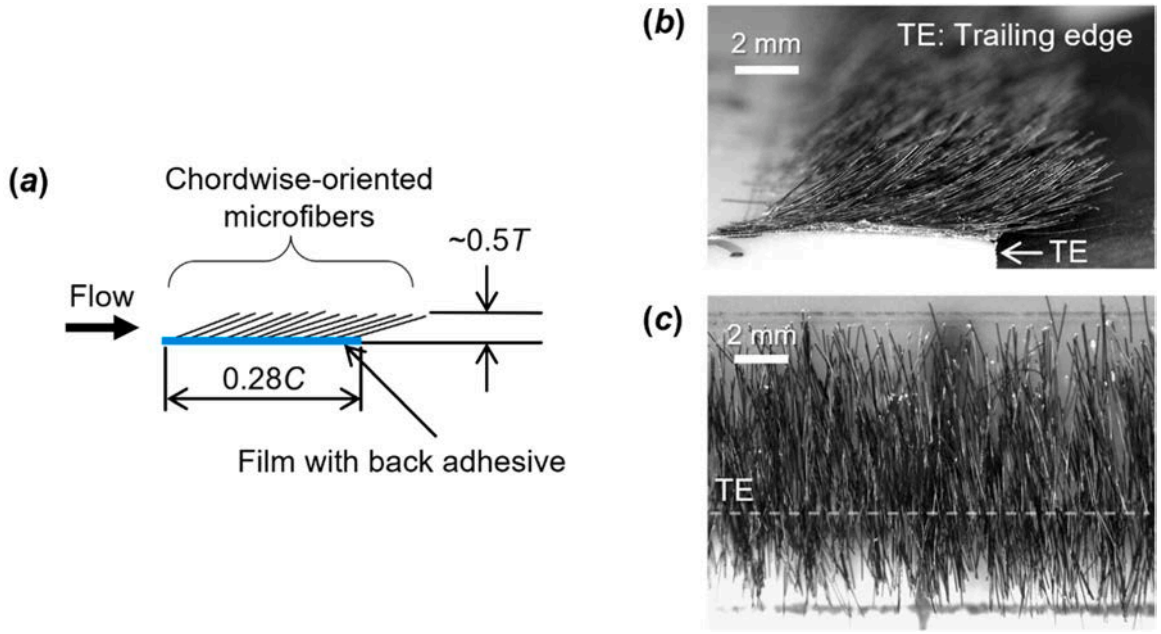

Fig. 4. (a) Schematic of the microfiber-coated strip seen from the lateral direction. In the schematic, the orientation angle and length of microfibers are exaggerated. (b) Microscopic image of lateral view of microfiber-coated strip applied on a blade. (c) Microscopic image of top view of microfiber-coated strip applied on a blade.

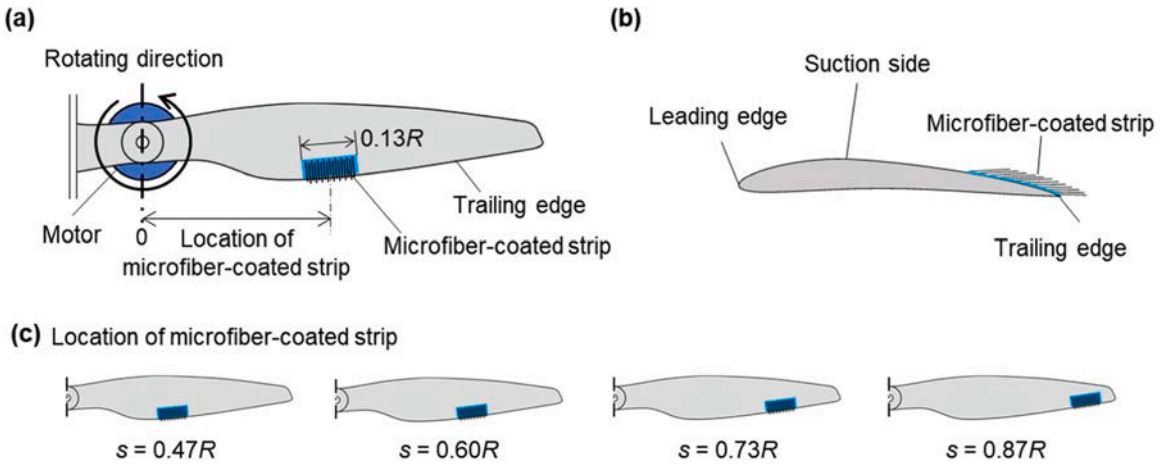

Fig. 5. Configuration of the microfiber-coated strips: (a) The propeller blade seen from the suction side; (b) Cross-sectional schematic of the propeller blade; and (c) Four different locations of the microfiber-coated strips. In the schematic the orientation angle and the length of microfibers and the shape of the airfoils are exaggerated.

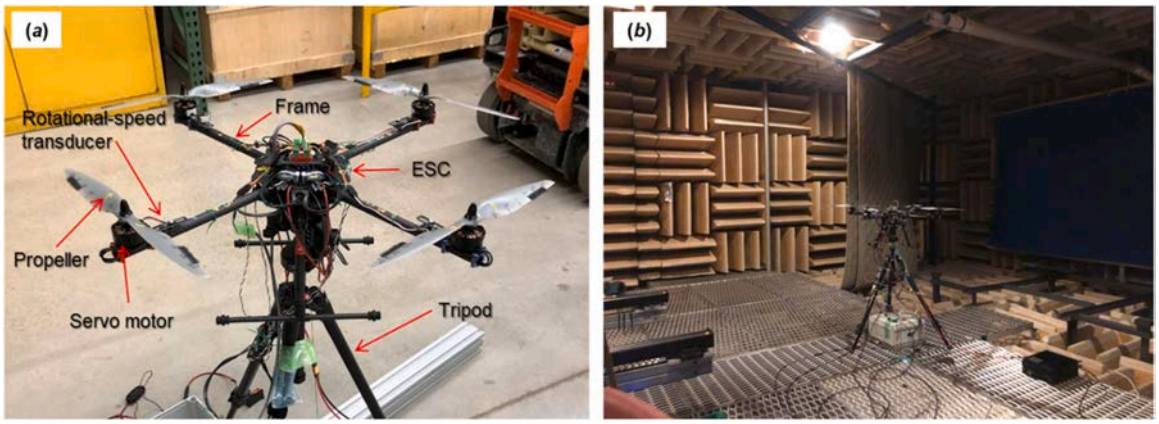

Fig. 6. Photographs of the quadcopter test stand: (a) Components of quadcopter test stand; (b) Quadcopter test stand housed in the anechoic chamber.

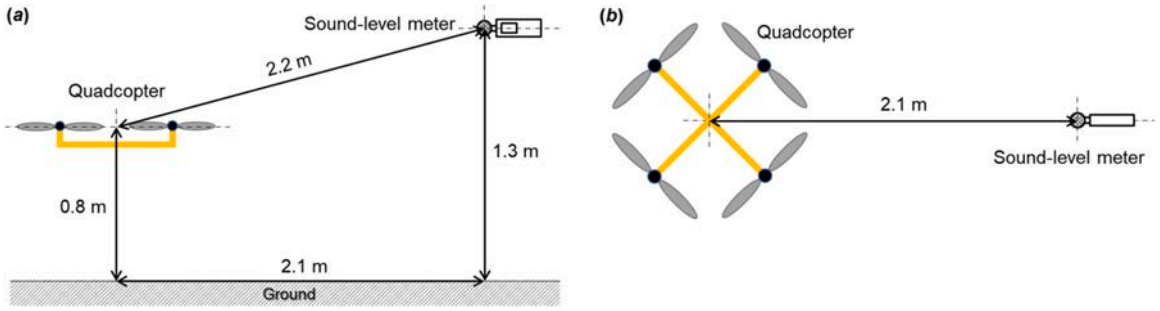

Fig. 7. Schematic description of sound level meter location: (a) Side view; and (b) Top view. Scale is exaggerated.

2.5. Propeller noise evaluation

The sound-level meter captured all the noise produced by the test setup which was comprised of the propeller noise, airframe noise, and motor noise generated by the operation of the quadcopter. To account for these various noise factors and extract the noise coming from the propeller, the differential time-weighted SPL, ΔSPL, between the microfiber-coated propeller and uncoated propeller was used. It is defined as:

$$\Delta SPL = SPL_m - SPL_u \quad (3)$$

where SPL_m and SPL_u are the time-weighted SPLs for the microfiber-coated propeller and the uncoated propeller, respectively. Negative ΔSPL shows a decrease in SPL compared to the uncoated propeller, while an increase in SPL is indicated by a positive ΔSPL.

3. Results and discussions

Fig. 8 shows the a-weighted and time-weighted SPL and the differential sound pressure level, ΔSPL, given in Eq. (3). The time-weighted SPL of the uncoated propeller, $SPL_u$was 67.2 dBA. The error bar shows the total error based on the standard deviation of the sampled data. A

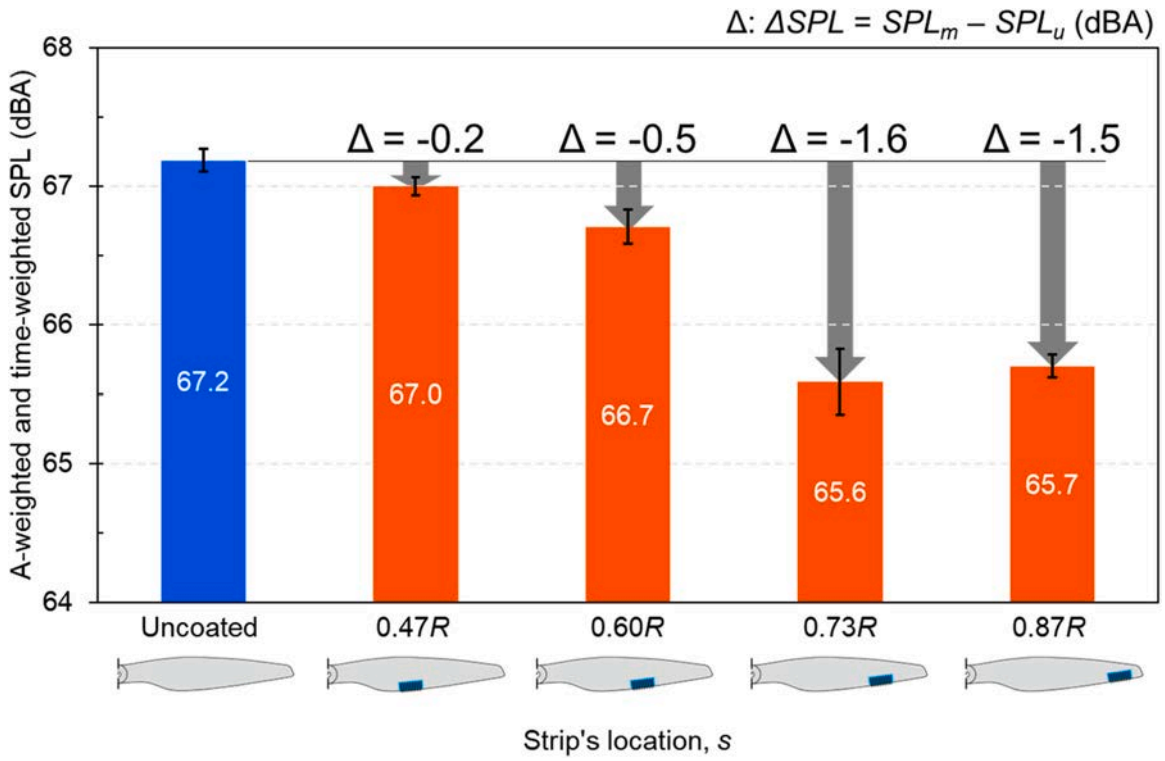

Fig. 8. The a-weighted and time-weighted SPL and the differential SPL, *ΔSPL*, between the microfiber-coated propeller and the uncoated propeller for different strip locations. Negative *ΔSPL* indicates a reduction of SPL compared to uncoated propeller. The error bar shows the total error based on the standard deviation of the sampled data.

negative *ΔSPL* was seen indicating that SPL was reduced compared to the uncoated propeller. The maximum reduction of 1.6 dBA was achieved at $s = 0.73\ R$. The microfiber-coated propeller demonstrated a reduction in the SPL for all strip locations. As hypothesized in Introduction, there is a location dependency of the microfiber coating in terms of noise reduction. As the microfiber-coated strip moved towards the blade-tip from $s = 0.47\ R$ to $s = 0.73\ R$, the microfiber-coated propeller enhanced the reduction of SPL from 0.2 dBA to 1.6 dBA. The reduction of SPLs at $s = 0.73\ R$ and $s = 0.87\ R$ were nearly identical within measurement uncertainty.

Fig. 9 shows the power spectral density (PSD) of the noise obtained by the sound-level meter, described in Section 2.4, of the uncoated propeller and the microfiber-coated propeller at $s = 0.73\ R$. This location was chosen as it corresponded to the maximum reduction in SPL. The peaks occurred at the blade passing frequency (BPF) and showed the tonal noise [32]. The peak due to BPF was captured around 98 Hz which corresponds to the frequency of the rotating propeller at 3000 rpm. The PSD of the microfiber-coated propeller was lower in amplitude in the range between 3 and 10 kHz compared to that of the uncoated propeller. At frequencies between 3 and 10 kHz, broadband noise with a hump

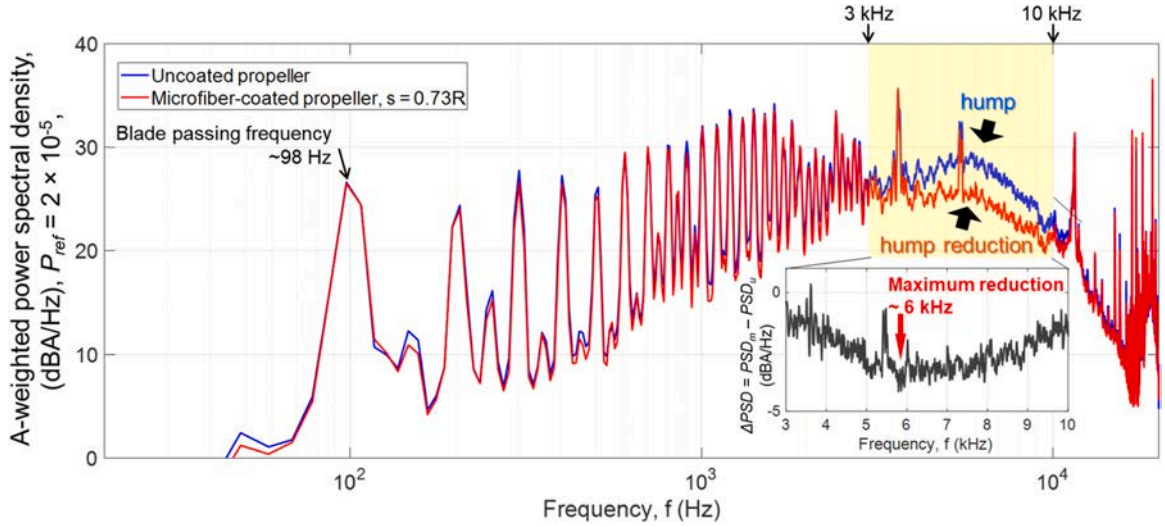

Fig. 9. A-weighted power spectral density (PSD) of the uncoated propeller and the microfiber-coated propeller at $s = 0.73\ R$, given in Eq. (2). The sub plot, *ΔPSD*, focuses on the frequencies between 3 and 10 kHz and shows the difference in PSD spectra between the microfiber-coated propeller and the uncoated propeller. Negative *ΔPSD* indicates a lower PSD for the microfiber-coated propeller compared to uncoated propeller in this range of frequencies.

dominates the spectrum [27,28,30,32–34]. It was found that the broadband noise hump was lower for the microfiber-coated propeller compared to the uncoated propeller. In the range below 3 kHz, no change in actual frequencies was seen in discrete peak frequencies accounting for tonal noise. The subplot in Fig. 9 shows the difference in PSD spectra, *ΔPSD*, between the microfiber-coated propeller and the uncoated propeller. The subplot focuses on the frequency range between 3 and 10 kHz. By looking at the differential between the power spectral densities, the frequency at which the maximum noise reduction occurred can be seen. Discrete spikes of both PSD spectra were seen around 3.6 and 5.4 kHz. Based on the uncertainty in the frequency resolution given in Section 2.4, these spikes are considered within uncertainty for the measurement. The maximum noise reduction can be seen around 6 kHz within the broadband noise.

The TBLTE and LBLVS noise described in the Chapter 1 are usually observed in the mid- to high-frequency range, which is typically from 1 to 30 kHz for small aerial vehicles [30,32–34]. The frequency range of the observed broadband-noise for this study was within that frequency range. LBLVS noise is not restricted to individual peaks, and instead is continuous across a range of frequencies. LBLVS can also generate broadband noise at a higher frequency range than the discrete frequency peaks observed in tonal noise [27,28,30,32–36]. LBLVS noise is associated with laminar flow that is separating from the surface (See Fig. 10 (a)) [7,23–25]. Especially, LBLVS noise associated with a laminar separation bubble is shown as a hump in broadband noise for low Reynolds number propellers [27,28,35,36]. The broadband hump around 6 kHz was shown and reduced by the microfiber-coated propeller (See Fig. 9). Based on the Reynolds number in this study, it can be assumed that boundary layer over the propeller was predominantly laminar. Thus, a laminar flow separation, transition, and a flow reattachment can occur as shown in Fig. 10 (a). The boundary layer becomes turbulent after flow reattachment [25]. Under the flow conditions in this study, the boundary layer at trailing edge can be considered predominantly turbulent. These observations support the idea that the observed broadband-noise is associated with the LBLVS noise or the LBLVS noise and the TBLTE noise. It suggests that the microfiber-coated propeller modifies flow features associated with the LBLVS noise or the LBLVS noise and TBLTE noise as shown in Fig. 10 (b).

A higher effectiveness of the microfiber-coated strip applied to the outer segment can be associated with the occurrence of a laminar flow separation at this location. Previous studies using similar propeller geometries and Reynolds number to this study have shown that the flow structure on the blade consists of laminar boundary layer, laminar flow separation, laminar separation bubble, flow reattachment, and turbulent boundary layer [35,36]. The noise source associated with a laminar separation bubble, turbulent flow after flow reattachment, or a separation with consequent vortex shedding, follows the laminar flow separation. These support that the effectiveness of the microfiber-coated strip applied to the outer segment is related to the noise associated with the laminar flow separation.

4. Conclusion

The increase in popularity of small aerial vehicles has created public health concerns surrounding propeller noise. To reduce this noise, the microfiber coating, a fibrous structure, was studied as a passive means of flow control and was applied to propeller blades of a quadcopter. The microfiber coating was placed coincident to the trailing edge of the propeller and its spanwise location was varied from 47 to 87% of the propeller radius. It was found that the propeller noise was dependent on the location of the microfiber-coated strip. The change in sound pressure level was a function of microfiber coating spanwise location. Compared

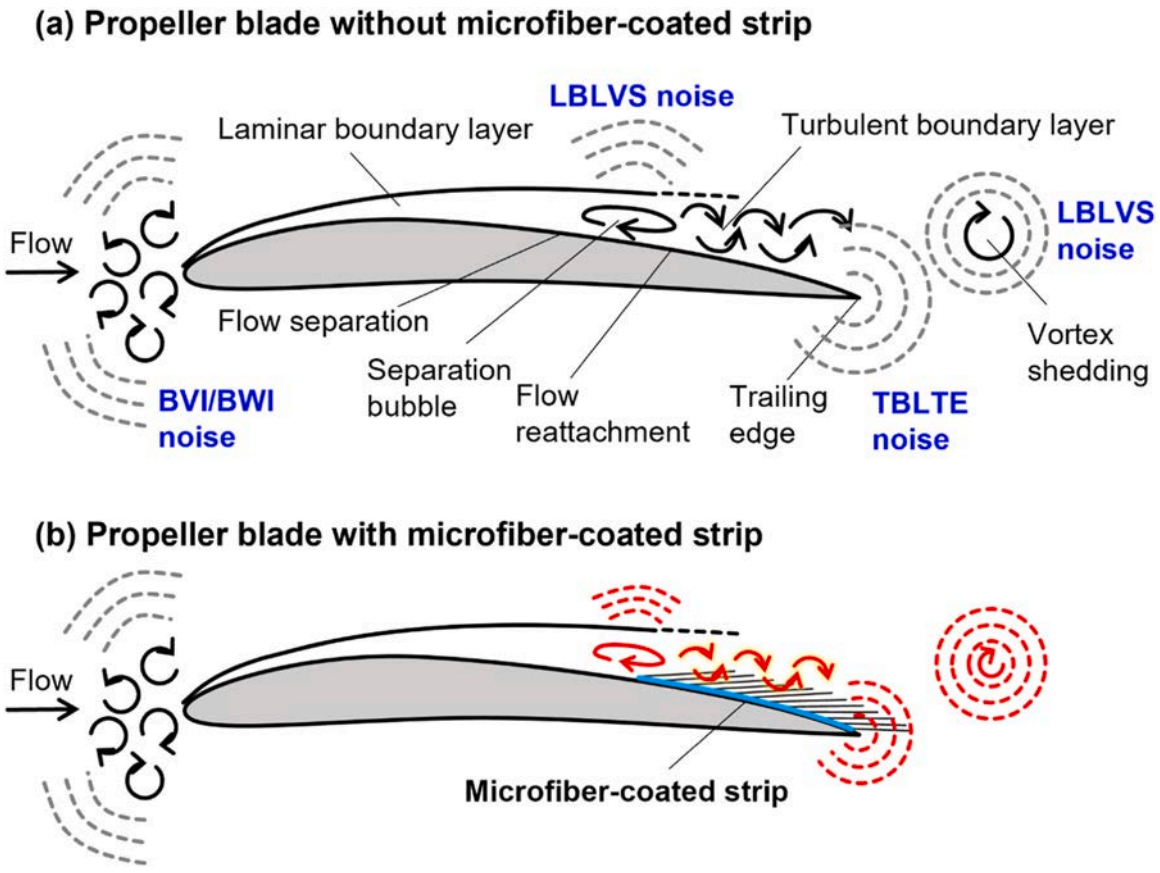

Fig. 10. Flow associated with noise sources: (a) Propeller blade without microfiber-coated strip; and (b) Propeller blade with microfiber-coated strip. In the schematic the orientation angle and the length of microfibers and the shape of the airfoils are exaggerated.

to the uncoated propeller, the maximum reduction in the sound pressure level for the microfiber-coated propeller was 1.6 dBA. This decrease in sound pressure level was achieved when the microfiber-coated strip was applied at 73% of the blade radius. The microfiber-coated propeller reduced the broadband noise hump in the frequency range between 3 and 10 kHz including a noise peak at ~6 kHz. The hump reduction is associated with the elimination or suppression of laminar boundary layer vortex-shedding noise for small aerial vehicles.

CRediT authorship contribution statement

Mitsugu Hasegawa: Writing – original draft, Methodology, Investigation, Formal analysis, Conceptualization. **Hirotaka Sakaue:** Writing – review & editing, Validation, Supervision, Methodology, Investigation, Formal analysis, Conceptualization.

Declaration of Competing Interest

The authors declare that they have no known competing financial interests or personal relationships that could have appeared to influence the work reported in this paper.

Data availability

Data will be made available on request.

Acknowledgements

Authors acknowledge Mr. Taro Tanaka, Mr. Masafumi Yamazaki, Mr. Daiki Kurihara and Mr. Joseph Gonzales for technical discussions.

References

[1] A. Christian, R. Cabell, Initial investigation into the psychoacoustic properties of small unmanned aerial system noise, in: Proceedings of the Twenty Third AIAA/CEAS Aeroacoustics Conference, 2017 (2017). https://doi.org/10.2514/6.2017-4051.
[2] D. Floreano, R.J. Wood, Science, technology and the future of small autonomous drones, Nature 521 (2015) 460–466, https://doi.org/10.1038/nature14542.
[3] A.J. Torija, Z. Li, R.H. Self, Effects of a hovering unmanned aerial vehicle on urban soundscapes perception, Transp. Res D. Transp. Environ. 78 (2020) 102195, https://doi.org/10.1016/J.TRD.2019.11.024.
[4] B. Schäffer, R. Pieren, K. Heutschi, J.M. Wunderli, S. Becker, Drone noise emission characteristics and noise effects on humans—a systematic review, Int. J. Environ. Res. Public Health 18 (2021) 5940, https://doi.org/10.3390/IJERPH18115940.
[5] M. Mulero-Pázmány, S. Jenni-Eiermann, N. Strebel, T. Sattler, J.J. Negro, Z. Tablado, Unmanned aircraft systems as a new source of disturbance for wildlife: a systematic review, PLoS One 12 (2017) e0178448, https://doi.org/10.1371/JOURNAL.PONE.0178448.
[6] M.A. Ditmer, J.B. Vincent, L.K. Werden, J.C. Tanner, T.G. Laske, P.A. Iaizzo, D. L. Garshelis, J.R. Fieberg, Bears show a physiological but limited behavioral response to unmanned aerial vehicles, Curr. Biol. 25 (2015) 2278–2283, https://doi.org/10.1016/J.CUB.2015.07.024.
[7] P. Candeloro, D. Ragni, T. Pagliaroli, Small-scale rotor aeroacoustics for drone propulsion: a review of noise sources and control strategies, Fluids 7 (2022) 279, https://doi.org/10.3390/fluids7080279.
[8] C. MN, UAS propeller/rotor sound pressure level reduction through leading edge modification, J. Appl. Mech. Eng. 6 (2017) 1–4, https://doi.org/10.4172/2168-9873.1000254.
[9] Y. Wei, F. Xu, S. Bian, D. Kong, Noise reduction of UAV using biomimetic propellers with varied morphologies leading-edge serration, J. Bionic Eng. 17 (2020) 767–779, https://doi.org/10.1007/S42235-020-0054-Z/METRICS.
[10] F. Avallone, W.C.P. Van Der Velden, D. Ragni, D. Casalino, Noise reduction mechanisms of sawtooth and combed-sawtooth trailing-edge serrations, J. Fluid Mech. 848 (2018) 560–591, https://doi.org/10.1017/JFM.2018.377.
[11] A. Cambray, E. Pang, S.A. Showkat Ali, D. Rezgui, M. Azarpeyvand, Investigation towards a better understanding of noise generation from UAV propellers, AIAA/CEAS Aeroacoustics Conf. 2018 (2018), https://doi.org/10.2514/6.2018-3450.
[12] R. Noda, T. Ikeda, T. Nakata, H. Liu, Characterization of the low-noise drone propeller with serrated Gurney flap, Front. Aerosp. Eng. 1 (2022) 8, https://doi.org/10.3389/FPACE.2022.1004828.
[13] H. Weger, M. Weger, M. Klaas, W. Schröder, Features of owl wings that promote silent flight, Interface Focus 7 (2017), https://doi.org/10.1098/RSFS.2016.0078.
[14] J.W. Jaworski, N. Peake, Aeroacoustics of silent owl flight, Annu Rev. Fluid Mech. 52 (2020) 395–420, https://doi.org/10.1146/annurev-fluid-010518-040436.
[15] R. Noda, T. Nakata, T. Ikeda, D. Chen, Y. Yoshinaga, K. Ishibashi, C. Rao, H. Liu, Development of bio-inspired low-noise propeller for a drone, J. Robot. Mechatron. 30 (2018) 337–343, https://doi.org/10.20965/JRM.2018.P0337.
[16] C. Teruna, F. Avallone, D. Casalino, D. Ragni, Numerical investigation of leading edge noise reduction on a rod-airfoil configuration using porous materials and serrations, J. Sound Vib. 494 (2021) 115880, https://doi.org/10.1016/J.JSV.2020.115880.
[17] C. Teruna, F. Avallone, D. Ragni, A. Rubio-Carpio, D. Casalino, Numerical analysis of a 3-D printed porous trailing edge for broadband noise reduction, J. Fluid Mech. 926 (2021) A17, https://doi.org/10.1017/JFM.2021.704.
[18] M. Hasegawa, H. Sakaue, Microfiber coating for drag reduction by flocking technology, Coatings 8 (2018) 464, https://doi.org/10.3390/coatings8120464.
[19] M. Hasegawa, H. Sakaue, Microfiber coating for flow control over a blunt surface, Coatings 9 (2019) 664, https://doi.org/10.3390/coatings9100664.
[20] M. Hasegawa, H. Sakaue, Experimental investigation of aerodynamic drag and flow characteristics of circular cylinder with microfiber coating, Exp. Therm. Fluid Sci. 129 (2021) 110478, https://doi.org/10.1016/j.expthermflusci.2021.110478.
[21] M. Nishimura, T. Kudo, M. Nishioka, Aerodynamic noise reducing techniques by using pile-fabrics, in: Proceedings of the Fifth AIAA/CEAS Aeroacoustics Conference and Exhibit (1999). https://doi.org/10.2514/6.1999-1847.
[22] M. Nishimura, T. Goto, Aerodynamic noise reduction by pile fabrics, Fluid Dyn. Res 42 (2010) 015003, https://doi.org/10.1088/0169-5983/42/1/015003.
[23] T.F. Brooks, J.R.Jr Jolly, M.A. Marcolini, Helicopter main-rotor noise: determination of source contributions using scaled model data, NASA Technical Paper TP-2825 (1988).
[24] G. Sinibaldi, L. Marino, Experimental analysis on the noise of propellers for small UAV, Appl. Acoust. 74 (2013) 79–88, https://doi.org/10.1016/J.APACOUST.2012.06.011.
[25] A. Leslie, K.C. Wong, D. Auld, Broadband Noise Reduction on a mini-UAV Propeller, in: Proceedings of the Fourteenth AIAA/CEAS Aeroacoustics Conference (Twenty Ninth AIAA Aeroacoustics Conference), American Institute of Aeronautics and Astronautics, Reston, Virigina, 2008. https://doi.org/10.2514/6.2008-3069.
[26] F. Petricelli, P. Chaitanya, S. Palleja-Cabre, S. Meloni, P.F. Joseph, A. Karimian, S. Palani, R. Camussi, An experimental investigation on the effect of in-flow distortions of propeller noise, Appl. Acoust. 214 (2023) 109682, https://doi.org/10.1016/J.APACOUST.2023.109682.
[27] S. Meloni, E. de Paola, E. Grande, D. Ragni, L.G. Stoica, A. Di Marco, R. Camussi, A wavelet-based separation method for tonal and broadband components of low Reynolds-number propeller noise, Meas. Sci. Technol. 34 (2023) 044007, https://doi.org/10.1088/1361-6501/ACB071.
[28] E. Grande, D. Ragni, F. Avallone, D. Casalino, Laminar separation bubble noise on a propeller operating at low Reynolds numbers, AIAA J. 60 (2022) 5324–5335, https://doi.org/10.2514/1.J061691/ASSET/IMAGES/LARGE/FIGURE17.JPEG.
[29] R.W. Deters, G.K. Ananda, M.S. Selig, Reynolds number effects on the performance of small-scale propellers, in: Proceedings of the Thirty Second AIAA Applied Aerodynamics Conference (2014). https://doi.org/10.2514/6.2014-2151.
[30] N.S. Zawodny, D.D.Jr Boyd, C.L. Burley, Acoustic characterization and prediction of representative, small-scale rotary-wing unmanned aircraft system components, in: Proceedings of the AHS Seventy Second Annual Forum, 2016: May 16-19.
[31] M. Hasegawa, H. Sakaue, Microfiber coating for flow control: effects on microfiber length in orientation control, Sens Actuators A Phys. 312 (2020) 112125, https://doi.org/10.1016/j.sna.2020.112125.
[32] N.A. Pettingill, N.S. Zawodny, C.S. Thurman, L.V. Lopes, Acoustic and performance characteristics of an ideally twisted rotor in hover, AIAA Scitech 2021 Forum (2021) 1–23, https://doi.org/10.2514/6.2021-1928.
[33] N. Intaratep, W.Nathan Alexander, W.J. Deveport, S.M. Grace, A. Dropkin, Experimental study of quadcopter acoustics and performance at static thrust conditions, in: Proceedings of the Twenty Second AIAA/CEAS Aeroacoustics Conference, 2016 (2016). https://doi.org/10.2514/6.2016-2873.
[34] Z. Huang, H. Yao, O. Sjögren, A. Lundbladh, L. Davidson, Aeroacoustic analysis of aerodynamically optimized joined-blade propeller for future electric aircraft at cruise and take-off, Aerosp. Sci. Technol. 107 (2020) 106336, https://doi.org/10.1016/J.AST.2020.106336.
[35] D. Casalino, G. Romani, R. Zhang, H. Chen, Lattice-Boltzmann calculations of rotor aeroacoustics in transitional boundary layer regime, Aerosp. Sci. Technol. 130 (2022) 107953, https://doi.org/10.1016/J.AST.2022.107953.
[36] D. Casalino, G. Romani, L.M. Pii, R. Colombo, Flow confinement effects on sUAS rotor noise, Aerosp. Sci. Technol. 143 (2023) 108756, https://doi.org/10.1016/J.AST.2023.108756.

Hirotaka Sakaue is an associate professor at the Department of Aerospace and Mechanical Engineering, University of Notre Dame. Prior to this, he was a researcher at Japan Aerospace Exploration Agency (JAXA). Dr. Sakaue received his MS and PhD degrees from School of Aeronautics and Astronautics, Purdue University, in 1999 and 2003, respectively. His research interests are in interdisciplinary studies on fluid mechanics and chemistry.

Mitsugu Hasegawa is a postdoctoral scholar at the Department of Aerospace and Mechanical Engineering, University of Notre Dame. He received his M.S. degree in mechanical engineering from Kanagawa Institute of Technology in 2015. He earned his PhD degree in aerospace engineering at University of Notre Dame in 2021. His research interests include the development of micro-structured surface and their applications to fluid mechanics.